Hindawi Publishing Corporation
International Journal of Photoenergy
Volume 2015, Article ID 594858, 9 pages
http://dx.doi.org/10.1155/2015/594858

Research Article

Design and Simulation of InGaN *p-n* Junction Solar Cell

A. Mesrane,[1] F. Rahmoune,[1] A. Mahrane,[2] and A. Oulebsir[3]

[1]*Laboratoire LIMOSE, Université M'hamed Bougara de Boumerdès, 35000 Boumerdès, Algeria*
[2]*Unité de Développement des Equipements Solaires (UDES), Centre de Développement des Energies Renouvelables (CDER), Route Nle No. 11, BP 386, Bou Ismaïl, 42415 Tipaza, Algeria*
[3]*Laboratoire d'Électronique Quantique, Faculté de Physique, USTHB, BP 32, El Alia, Bab Ezzouar, 16111 Alger, Algeria*

Correspondence should be addressed to A. Mesrane; mesranefatah@gmail.com

Received 21 March 2015; Revised 17 May 2015; Accepted 17 June 2015

Academic Editor: Elias Stathatos

The tunability of the InGaN band gap energy over a wide range provides a good spectral match to sunlight, making it a suitable material for photovoltaic solar cells. The main objective of this work is to design and simulate the optimal InGaN single-junction solar cell. For more accurate results and best configuration, the optical properties and the physical models such as the Fermi-Dirac statistics, Auger and Shockley-Read-Hall recombination, and the doping and temperature-dependent mobility model were taken into account in simulations. The single-junction $In_{0.622}Ga_{0.378}N$ (Eg = 1.39 eV) solar cell is the optimal structure found. It exhibits, under normalized conditions (AM1.5G, 0.1 W/cm^2, and 300 K), the following electrical parameters: J_{sc} = 32.6791 mA/cm^2, V_{oc} = 0.94091 volts, FF = 86.2343%, and η = 26.5056%. It was noticed that the minority carrier lifetime and the surface recombination velocity have an important effect on the solar cell performance. Furthermore, the investigation results show that the $In_{0.622}Ga_{0.378}N$ solar cell efficiency was inversely proportional with the temperature.

1. Introduction

Recently, various studies on solar cells using III-nitrides semiconductors in the photovoltaic applications have been done. Among them the InGaN alloy is a promising candidate for the photovoltaic applications because it exhibits attractive photovoltaic properties such as high tolerance to radiation, high mobility, and large absorption coefficient allowing thinner layers of material to absorb most of the solar spectrum [1].

Moreover, the most important advantage of InGaN alloy might be the direct band gap energy which can be adjusted according to the indium composition. Thus, the InGaN's energy band gap can be tuned from 0.7 eV to 3.42 eV, covering approximately the total solar spectrum.

The layers of InGaN solar cell can be deposited using the cost effective techniques, such as Metal Organic Chemical Vapor Deposition (MOCVD), Metal Organic Vapor Phase Epitaxy (MOVPE), and Molecular Beam Epitaxy (MBE) [2]. Whatever the deposition technique used, higher growth rates (~1.0 Angstrom/second) and lower temperature (~550°C) characterize the InGaN growth [3].

In 2007, Zhang et al. have modeled the performance of $In_{0.65}Ga_{0.35}N$ single-junction solar cell and achieved a conversion efficiency of 20.284% [4]. In 2008, Shen et al. have obtained for the similar $In_{0.65}Ga_{0.35}N$ solar cell higher efficiency (24.95%) due to the adoption of the density of states (DOS) model, providing much more information about recombination/generation in semiconductors than the lifetime model, and neglecting the defect effects [5]. The InGaN-based solar cell modeled by Bouzid and Ben Machiche [6], for a fraction of composition of indium (x = 0.53), has reached 24.88% conversion efficiency. The same solar cell was improved by [7] attaining 25.16% efficiency. Benmoussa et al. have simulated $In_{0.52}Ga_{0.48}N$ using AMPS-1D software and published 22.99% efficiency in 2013 [8]. Recently, in 2014, $In_{0.64}Ga_{0.36}N$ single-junction solar cell was designed and numerically optimized by Akter, exhibiting a high efficiency of 25.02% [2].

The different yields obtained in the works cited above can be principally attributed to the different optical properties, physical parameters, and band gap energy used for each solar cell studied. Thus, the obtained conversion efficiencies for

InGaN solar cells with a band gap energy of 1.32 eV [5], 1.34 eV [2], 1.622 eV [7], and 1.64 eV [8] are, respectively, 24.95%, 25.02%, 25.16%, and 22.99%.

Given that the band gap energy of about 1.39 eV permits a single-junction solar cell to achieve theoretically the maximum conversion efficiency of ~31% [9, 10], we have opted in our study for $In_xGa_{1-x}N$-based single-junction solar cell with a fraction composition of indium of $x = 0.622$.

In contrast with the previous work [4–8], we have simulated the $In_xGa_{1-x}N$-based single-junction solar cell with the optimum band gap energy of 1.39 eV, using the optical and physical properties of $In_{0.622}Ga_{0.378}N$ and taking into account the Auger and SRH recombination. Furthermore, we have adopted an appropriate carrier mobility model which takes into account the doping concentration, the temperature, and the material composition, which was different from previous work where the carrier mobility in $In_xGa_{1-x}N$ was considered similar to GaN and depending only on doping concentration.

The aim of this simulation work is to obtain the maximum conversion efficiency of $In_{0.622}Ga_{0.378}N$ (1.39 eV) single-junction solar cell with the best structure parameters. The effects of the concentration doping and the thickness of each layer on the electrical parameters of the solar cell, such as the short circuit current density (J_{sc}), the open circuit voltage (V_{oc}), the fill factor (FF), and the conversion efficiency (η), were investigated. Furthermore, the effects of the minority carrier lifetime and the surface recombination velocity on the conversion efficiency of the single-junction $In_{0.622}Ga_{0.378}N$ solar cell were also studied.

Finally, the behavior of the electrical characteristics of the solar cell versus the temperature has been studied.

2. Modelling and Simulation

2.1. Structure. As the numerical simulation is an important way to explore the possibility of a new solar cell structure, the $In_{0.622}Ga_{0.378}N$ *p-n* single-junction solar cells have been studied using two-dimensional numerical computer simulation tool (ATLAS from Silvaco).

Atlas is a physically based two- and three-dimensional device simulator. It predicts the electrical behavior of specified semiconductor structures [11].

All the simulations were performed under normalized conditions that are 1 sun, a temperature of 300 K, and AM1.5 illumination. The antireflecting layer is considered as perfect without reflection losses.

The $In_{0.622}Ga_{0.378}N$ single-junction solar cell structure studied consists of a P-type emitter and N-type base, as shown in Figure 1.

2.2. Electrical Parameters Calculation. The density of the total photocurrent drawn from the *p-n* junction solar cell at a given wavelength is the sum of the photocurrent densities collected from each layer of the *p-n* junction and is given by [12, 13] as follows:

$$J_{ph} = J_n + J_p + J_{dr}, \tag{1}$$

$$J_n = \left(\frac{qF(1-R)\alpha L_n}{\alpha^2 L_n^2 - 1}\right)\left(\frac{(S_n\tau_n/L_n + \alpha L_n) - e^{-\alpha x_j}\left((S_n\tau_n/L_n)\cosh\left(x_j/L_n\right) + \sinh\left(x_j/L_n\right)\right)}{(S_n\tau_n/L_n)\sinh\left(x_j/L_n\right) + \cosh\left(x_j/L_n\right)} - \alpha L_n e^{-\alpha x_j}\right), \tag{2}$$

$$J_p = \left(\frac{qF(1-R)\alpha L_p}{\alpha^2 L_p^2 - 1}e^{-\alpha(x_j+W)}\right)\left(\alpha L_p - \frac{(S_p\tau_p/L_p)\left(\cosh\left(H/L_p\right) - e^{-\alpha H}\right) + \sinh\left(H/L_p\right) + \alpha L_p e^{-\alpha H}}{(S_p\tau_p/L_p)\sinh\left(H/L_p\right) + \cosh\left(H/L_p\right)}\right), \tag{3}$$

where J_n and J_p are the photocurrent densities due to electrons and holes collected, respectively, at the depletion edges x_j and $x_j + W$. q is the electron charge, F is the density of the incident photon flux per unit bandwidth, R is the device reflectance, and α is the absorption coefficient. $L_{n,h}$, $S_{n,h}$, and $\tau_{n,h}$ are the minority carrier diffusion length, surface recombination velocity, and lifetime, respectively, in p-layer and n-layer. x_j, W, and H are the junction depth, the depletion region width, and the neutral thicknesses of the N-type region, respectively.

As the quantum efficiency in the space charge region is close to 100%, all the absorbed photons contribute to the photocurrent [13]. Thus, the photocurrent density collected from the depletion region is given by [12, 13] as follows:

$$J_{dr} = qF(1-R)e^{-\alpha x_j}\left(1 - e^{-\alpha W}\right). \tag{4}$$

The surface recombination, the open circuit voltage, and the reverse saturation current density are given by the following expressions [14, 15]:

$$V_{oc} = \frac{K_B \cdot T}{q}\ln\left(\frac{J_{sc}}{J_0} + 1\right), \tag{5}$$

$$J_0 = qn_i^2 \cdot \frac{L_n}{\tau_n N_A}\left(\frac{(S_n\tau_n/L_n)\cosh\left(x_j/L_n\right) + \sinh\left(x_j/L_n\right)}{(S_n\tau_n/L_n)\sinh\left(x_j/L_n\right) + \cosh\left(x_j/L_n\right)}\right) + qn_i^2 \cdot \frac{L_p}{\tau_p N_D}\left(\frac{(S_p\tau_p/L_p)\cosh\left(H/L_p\right) + \sinh\left(H/L_p\right)}{(S_p\tau_p/L_p)\sinh\left(H/L_p\right) + \cosh\left(H/L_p\right)}\right), \tag{6}$$

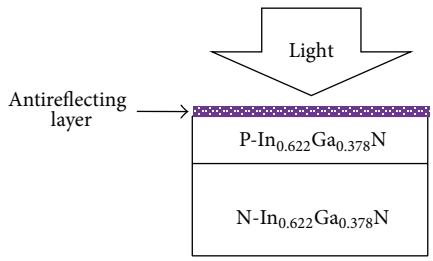

Figure 1: $In_{0.622}Ga_{0.378}N$ single-junction solar cell structure.

where V_{oc} is the open circuit voltage, J_{sc} is the short circuit current density, and J_0 is the reverse saturation current density. K_B and T are Boltzmann's constant and the lattice temperature, respectively. N_A and N_D are the initial acceptor and donor doping concentrations, respectively. n_i is the intrinsic carrier concentration, which is expressed as

$$n_i^2 = N_C N_V e^{-E_g/K_B T}, \tag{7}$$

where N_C and N_V are the effective densities of states in the conduction and valence band, respectively. E_g is the band gap energy.

The conversion efficiency of the solar cell is given by the following equation [15]:

$$\eta\,(\%) = \frac{I_{sc} \cdot V_{oc} \cdot \mathrm{FF}}{P_{in}}, \tag{8}$$

where P_{in} is the incident power of the solar spectrum, I_{sc} is the short circuit current, and FF is the fill factor of the solar cell.

2.3. Physical and Optical Parameters. The single-junction solar cell used in our study is based on $In_{0.622}Ga_{0.378}N$ alloy with a band gap energy of 1.39 eV, which is related to the indium composition fraction (x) at a temperature of 300 K by [7, 16]:

$$E_g\left(In_xGa_{1-x}N\right) = x \cdot E_g^{InN} + (1-x) \cdot E_g^{GaN} - b \cdot x \cdot (1-x), \tag{9}$$

where the band gap energy of InN (E_g^{InN}) and GaN (E_g^{GaN}) is 0.7 eV and 3.42 eV, respectively. x is the indium content and b is the bowing parameter ($b = 1.43$) [7, 16].

The dependence of the energy band gap to the temperature is modeled in the Atlas software as follows [11]:

$$E_g\left(T_L\right) = E_{g300}\left(In_xGa_{1-x}N\right) + E_{g\alpha}\left[\frac{300^2}{300 + E_{g\beta}} - \frac{T_L^2}{T_L + E_{g\beta}}\right], \tag{10}$$

where E_{g300} is given by (1). $E_{g\alpha}$ and $E_{g\beta}$ are the parameters related to the materials used in the single junction. They are set, respectively, at 9.09×10^{-4} eV·K^{-1} and 650 K [11] and are valid for the whole composition range of $In_xGa_{1-x}N$.

The other modeling parameters of the $In_xGa_{1-x}N$ alloy were calculated using the following equations.

Table 1: Nitride low field mobility model parameter values [18].

Material	$U_{max,n}$ (cm^2/V·s)	$U_{min,n}$ (cm^2/V·s)
InN	3138.4	774
$In_{0.8}Ga_{0.2}N$	1252.7	644.3
$In_{0.5}Ga_{0.5}N$	758.1	459.4
$In_{0.2}Ga_{0.8}N$	684.2	389.4
GaN	1460.7	295

Electron Affinity (χ) [4, 8, 17]:

$$\chi\left(In_xGa_{1-x}N\right) = 4.1 + 0.7\left(3.4 - E_g\right). \tag{11}$$

Relative permittivity (ε) [16]:

$$\varepsilon\left(In_xGa_{1-x}N\right) = 15.3x + 8.9\,(1-x). \tag{12}$$

Effective density of states in the conduction band (N_C) [8, 17]:

$$N_C\left(In_xGa_{1-x}N\right) = (0.9x + 2.3\,(1-x)) \cdot 10^{18}. \tag{13}$$

Effective density of states in the valence band (N_V) [8, 17]:

$$N_V\left(In_xGa_{1-x}N\right) = (5.3x + 1.8\,(1-x)) \cdot 10^{19}. \tag{14}$$

Effective masses (m_n/m_h) [11]:

$$m_n\left(In_xGa_{1-x}N\right) = 0.12x + 0.2\,(1-x),$$
$$m_h\left(In_xGa_{1-x}N\right) = 0.17x + 1.0\,(1-x). \tag{15}$$

The low field mobility model developed by Farahmand et al. [18] has also been used in order to study the hole and the electron mobility behavior in the $In_xGa_{1-x}N$ alloy depending on the material composition and the temperature. The electron or hole mobility is given by the following expression [18]:

$$U_0\,(N,T) = U_{min,i}\left(\frac{T}{300}\right)^{B1} + \frac{\left(U_{max,i} - U_{min,i}\right)(T/300)^{B2}}{1 + \left(N/N\mathrm{ref}\,(T/300)^{B3}\right)^{\gamma(T/300)^{B4}}}, \tag{16}$$

where N is the total doping of the layer and Nref is the doping of the substrate which is fixed at 10^{17} cm^{-3}. $B1$, $B2$, $B3$, $B4$, and γ are the specific parameters for a given material.

U_{min} and U_{max}, the values for the carrier mobility, are given in Table 1.

For other composition fractions not listed in Table 1, $In_xGa_{1-x}N$ electron mobility was got by a linear interpolation from the nearest composition fractions. As the experimental data for the hole mobility in the InGaN alloys are not available, we have assumed that the hole mobility in $In_xGa_{1-x}N$ is the same as in GaN [6, 7].

Table 2: Fitting parameters used to calculate the absorption coefficient of the $In_xGa_{1-x}N$ alloys [19].

Indium composition	C	D
1	0.69642	0.46055
0.83	0.66796	0.68886
0.69	0.58108	0.66902
0.57	0.60946	0.62182
0.5	0.51672	0.46836
0	3.52517	−0.65710

The InGaN alloys absorption coefficient α is given by [16, 19]:

$$\alpha\left(In_xGa_{1-x}N\right) = 10^5\sqrt{C\left(E_{ph}-E_g\right)+D\left(E_{ph}-E_g\right)^2}, \quad (17)$$

where E_{ph} is the photon energy and C and D, given in Table 2, are parameters dependent on the alloy composition.

For the $In_xGa_{1-x}N$ alloys, Adachi's wavelength-dependent refractive index model is given by the following equation [16, 20]:

$$n(E) = \sqrt{A\left(\frac{E_{ph}}{E_g}\right)^{-2}\left\{2-\sqrt{1+\frac{E_{ph}}{E_g}}-\sqrt{1-\frac{E_{ph}}{E_g}}\right\}+B}, \quad (18)$$

where A and B depend on the material composition. In the case of the $In_xGa_{1-x}N$ alloy, A and B are given by the following equation [16]:

$$A\left(In_xGa_{1-x}N\right) = 13.55x + 9.31(1-x),$$
$$B\left(In_xGa_{1-x}N\right) = 02.05x + 3.03(1-x). \quad (19)$$

In order to take into account the action of several physical phenomena that take place in the structure, the following physical models have also been implemented:

(i) the doping and temperature-dependent mobility models;

(ii) the Auger recombination models;

(iii) the Shockley-Read-Hall recombination models;

(iv) the Fermi-Dirac statistics.

Some assumptions have been made to simplify the simulations. Thus, the Auger recombination coefficients for both electrons and holes, for the $In_xGa_{1-x}N$ alloys, are set at 1.5×10^{-30} $cm^6 \cdot s^{-1}$ [16]. As the hole lifetimes of GaN and InN are, respectively, 6.5 ns and 5.4 ns [7, 19], the $In_xGa_{1-x}N$ alloys have probably lower minority carrier lifetimes, and hence the electrons and holes lifetimes were assumed to be 1 ns [16, 19].

The surface recombination velocities of the minorities (electrons or holes) were taken to be 10^3 $cm \cdot s^{-1}$ [4, 5, 7].

Table 3: Initial physical and geometrical parameters.

Parameters	Values
E_g (eV)	1.39
N_A (cm^{-3})	$5 \cdot 10^{17}$
N_D (cm^{-3})	$5 \cdot 10^{17}$
$\tau_{n,h}$ (ns)	1.00
$S_{n,h}$ ($cm \cdot s^{-1}$)	10^3
d (μm)	4.00

d is approximately the proper total thickness of the $In_{0.622}Ga_{0.378}N$ single-junction solar cell (~3.918 μm).

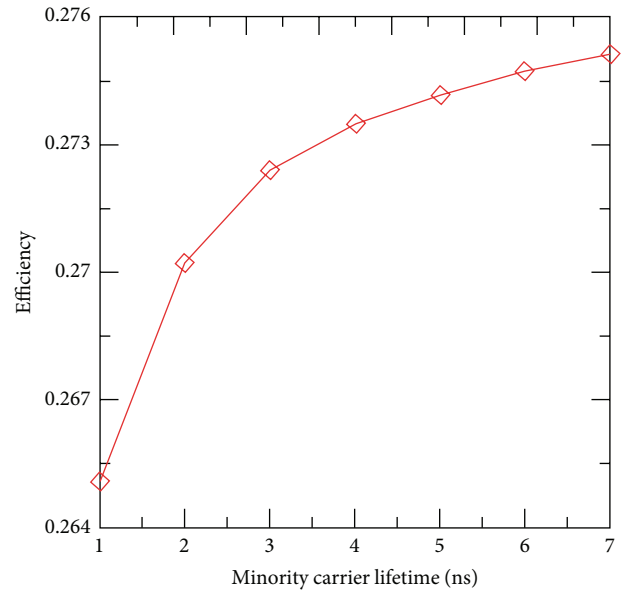

Figure 2: $In_{0.622}Ga_{0.378}N$ efficiency versus minority carrier lifetimes.

3. Results and Discussion

For the case studied, the initial physical and geometrical parameter values used for the single-junction $In_{0.622}Ga_{0.378}N$ solar cell are presented in Table 3.

The dependence of the $In_{0.622}Ga_{0.378}N$ single-junction solar cell conversion efficiency on the minority carrier lifetimes and the surface recombination velocities was investigated.

3.1. Effect of Minority Carrier Lifetimes on $In_{0.622}Ga_{0.378}N$ Conversion Efficiency. Assuming that the surface recombination velocity was set at 10^3 cm/s, the conversion efficiency of $In_{0.622}Ga_{0.378}N$ single-junction solar cell was determined for different values of minority carrier lifetimes as shown in Figure 2.

The results of simulations show that the conversion efficiency increases with the minority carrier (electrons/holes) lifetimes. According to (1)–(6) and (8), this is due to the low defect density that leads to the increase of the photocurrent density and the decrease of the reverse saturation current density inducing the enhancement of the open circuit voltage and so the conversion efficiency.

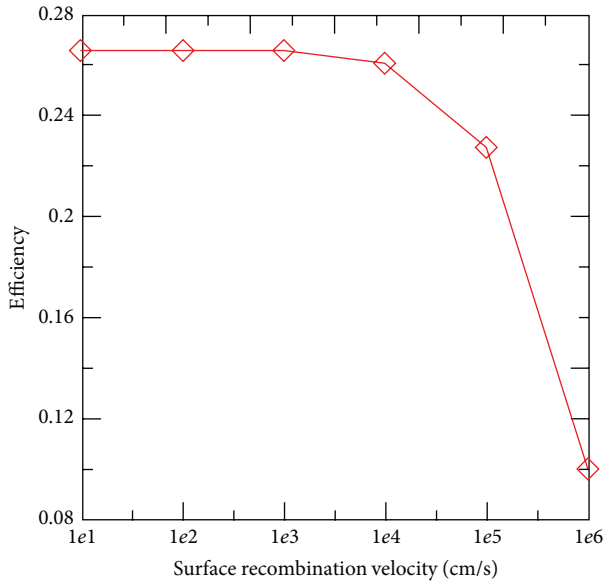

FIGURE 3: $In_{0.622}Ga_{0.378}N$ efficiency versus surface recombination velocities.

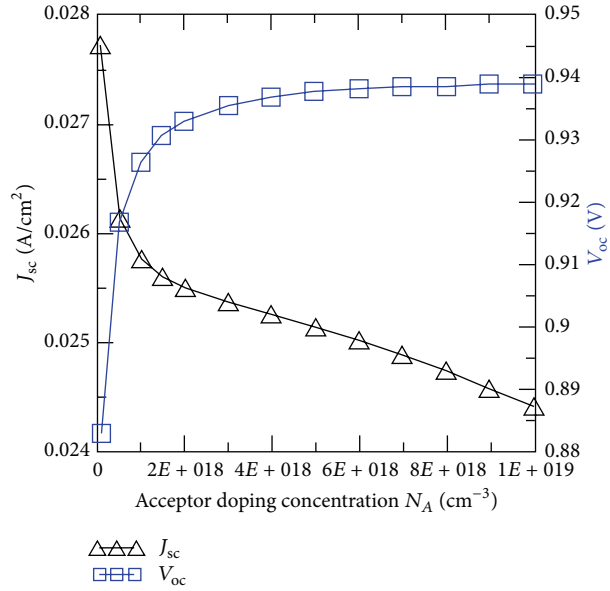

FIGURE 4: The short circuit current density and the open circuit voltage versus the acceptor doping concentration N_A.

3.2. Effect of Surface Recombination Velocities on $In_{0.622}Ga_{0.378}N$ Conversion Efficiency. Given that the minority carrier lifetimes were set at 1 ns, the influence of the surface recombination velocity on the $In_{0.622}Ga_{0.378}N$ single-junction solar cell efficiency was presented in Figure 3.

We notice that when the surface recombination velocities exceed 10^3 cm·s^{-1}, the single-junction $In_{0.622}Ga_{0.378}N$ solar cell efficiency decreases heavily due to the high dropping in photogenerated carrier collection by the electrodes. In fact, according to (1)–(6) and (8), the increase of the surface recombination velocity, due to the high surface defect density, conducts to the decrease of the photocurrent density and the open circuit voltage, via the increasing reverse saturation current which is directly proportional to the defect density, and this results in the decrease of the conversion efficiency.

To get the best $In_{0.622}Ga_{0.378}N$ single-junction solar cell configuration, a great number of simulations were done to select the optimal device parameters as the optimal doping concentration and the optimal thickness of each layer of the solar cell.

3.3. Optimal Doping Concentration of the Front Layer. The doping concentration of the front layer has an effect on the number of the photogenerated carriers which has a consequence on the short circuit current density, the open circuit voltage, the maximal power, and the conversion efficiency. To study this effect, we have varied the acceptor doping concentration N_A from 10^{17} cm^{-3} to 10^{19} cm^{-3}.

As shown by Figure 4, when the acceptor doping concentration N_A decreases, the carrier mobility and the minority carrier lifetime increase, inducing an enhancement in the minority carrier diffusion length and better collection efficiency, resulting in the improvement of the current density. According to (5) and (6), the reverse saturation current density decreases with the increasing of the doping concentration, inducing the increase of the open circuit current.

As shown in Figure 5, while the doping concentration N_A increases, the maximal power produced by the solar cell and its conversion efficiency increase first and then decrease. The optimum efficiency of $In_{0.622}Ga_{0.378}N$ single-junction solar cell was reached when the acceptor doping concentration was 1.5×10^{18} cm^{-3}.

3.4. Optimal Thickness of the Front Layer. Since the optimal acceptor doping concentration was found, the main electrical parameters (J_{sc}, η) of the solar cell were calculated for a range of p-layer thickness comprised between 0.01 and 1 μm.

As shown in Figures 6 and 7, with the increasing of the front layer thickness of the single-junction $In_{0.622}Ga_{0.378}N$ solar cell, the short circuit current density (J_{sc}) and the conversion efficiency (η) increase, first, and then decrease.

When the front layer thickness decreases, the distance between the space charge region and the surface decreases, which improves the effective collection efficiency inducing the enhancement of the short circuit current density. At the same time, if the surface recombination was taken into account, the collection efficiency of the depletion region will be weakened as this last is too close to the surface. The reduction of the collection efficiency leads to the decrease of the short circuit current density and the conversion efficiency.

Figure 6 shows that the peak of the short circuit current density was reached for a front layer thickness of 0.03 μm.

As shown in Figure 7, for a front layer thickness of 0.25 μm, the $In_{0.622}Ga_{0.378}N$ single-junction solar cell reaches the best conversion efficiency.

3.5. Optimal Thickness of the Back Layer. In this part, we have determined the conversion efficiency of the $In_{0.622}Ga_{0.378}N$

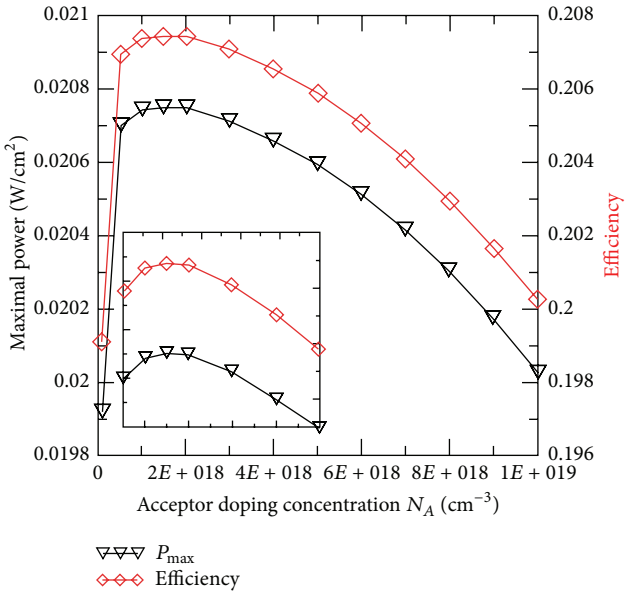

FIGURE 5: The maximal power and the solar cell efficiency versus the acceptor doping concentration N_A.

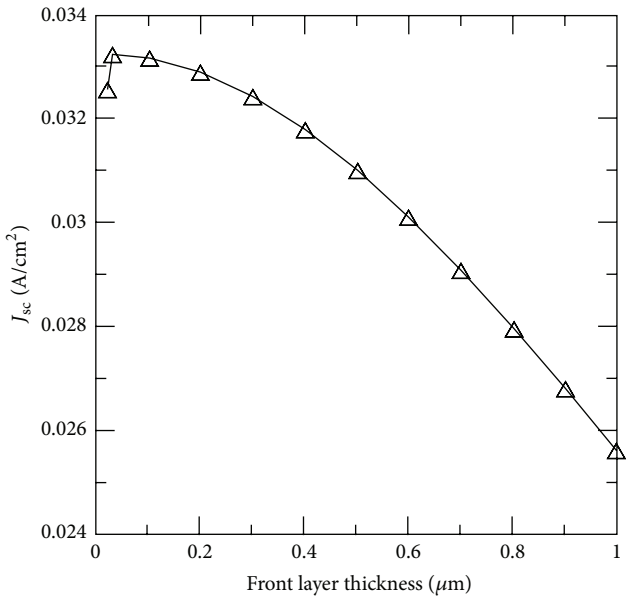

FIGURE 6: Short circuit current density versus the front layer thickness.

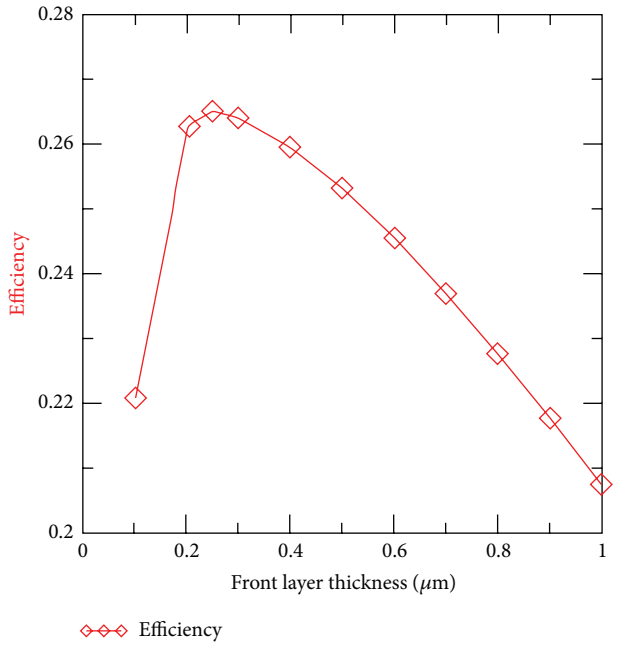

FIGURE 7: Calculated efficiency versus the front layer thickness.

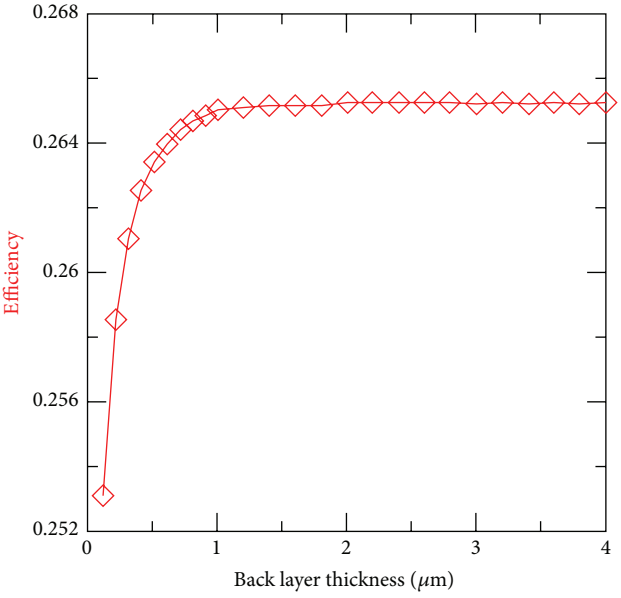

FIGURE 8: Calculated efficiency versus the back layer thickness.

single-junction solar cell when varying the N-layer thickness as illustrated in Figure 8.

We notice that the conversion efficiency is enhanced with the increase of the back layer thickness until 1 μm, but beyond 1 μm it remains almost constant at 26.50%. Therefore, the electrical parameters of the $In_{0.622}Ga_{0.378}N$ solar cell are less affected by the back layer thickness than the front layer thickness.

3.6. Optimal Performance of $In_{0.622}Ga_{0.378}N$ SJ Solar Cell. The optimal structure obtained from our investigations for the $In_{0.622}Ga_{0.378}N$ single-junction solar cell was 0.25 μm P-layer thickness and 1.0 μm N-layer thickness, with acceptor and donor doping concentrations of 1.5×10^{18} cm^{-3} and 5×10^{17} cm^{-3}, respectively.

The calculated electrical parameters, the *I-V* and *P-V* characteristics of the final $In_{0.622}Ga_{0.378}N$ single-junction solar cell structure, under normalized conditions, were presented, respectively, in Table 4 and Figure 9.

Table 4: Calculated parameters of the $In_{0.622}Ga_{0.378}N$ SJ solar cell under AM1.5G, 0.1 W/cm^2, and 300 K.

PV parameters	Values
J_{sc} (mA/cm^2)	32.6791
V_{oc} (volts)	0.94091
P_{max} (mW/cm^2)	26.5154
FF (%)	86.2334
η (%)	26.5056

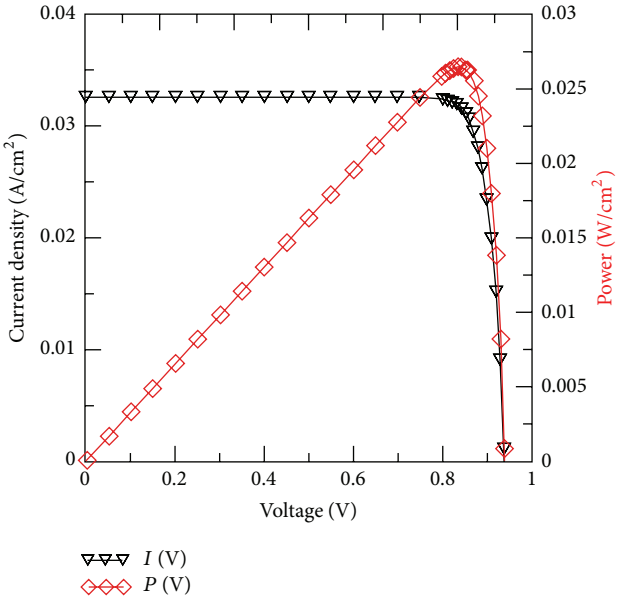

Figure 9: $I(V)$ and $P(V)$ characteristic for the optimal $In_{0.622}Ga_{0.378}N$ SJ solar cell configuration.

3.7. The Temperature Dependence of $In_{0.622}Ga_{0.378}N$ SJ Solar Cell. As the temperature has a great impact on the solar cell operation, we have studied its behavior through the variation of its electrical parameters versus the temperature.

The temperature was varied from 280 K to 400 K as presented in Figure 10.

As shown in Figure 10, the electrical characteristic I-V of the $In_{0.622}Ga_{0.378}N$ solar cell varies with the temperature. Indeed, while the short circuit current density (J_{sc}) increases slightly with the temperature, the open circuit voltage (V_{oc}) decreases strongly, inducing the degradation of the conversion efficiency as illustrated in Figure 11.

The high reduction of the open circuit voltage with the increased temperature was caused by the reduction of the band gap energy and the extreme increase of the reverse saturation current density, which is very sensitive with temperature, as illustrated in Figure 12.

According to (6) and (7), the reverse saturation current density increases exponentially with increasing temperature, via the exponential dependence of the intrinsic carrier concentration with the temperature.

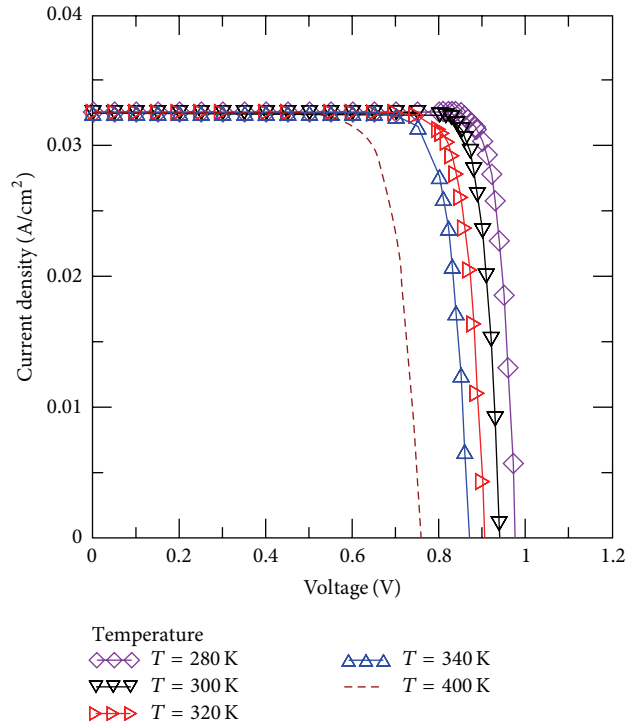

Figure 10: Current-voltage characteristics of $In_{0.622}Ga_{0.378}N$ solar cell versus temperature.

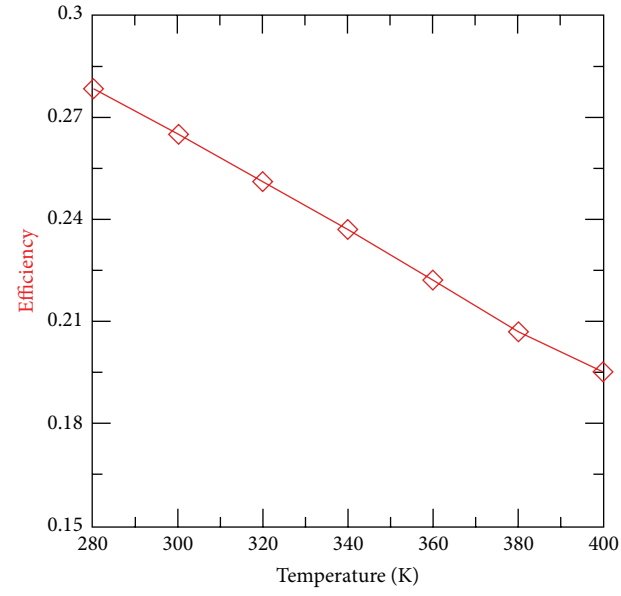

Figure 11: $In_{0.622}Ga_{0.378}N$ solar cell efficiency versus temperature.

4. Conclusion

The calculation of the photovoltaic parameters of the $In_{0.622}Ga_{0.378}N$ p-n single-junction solar cell, for the cases of different doping concentrations and different thicknesses of each layer, has allowed achieving the best solar cell structure with optimum performance. It was found that the solar

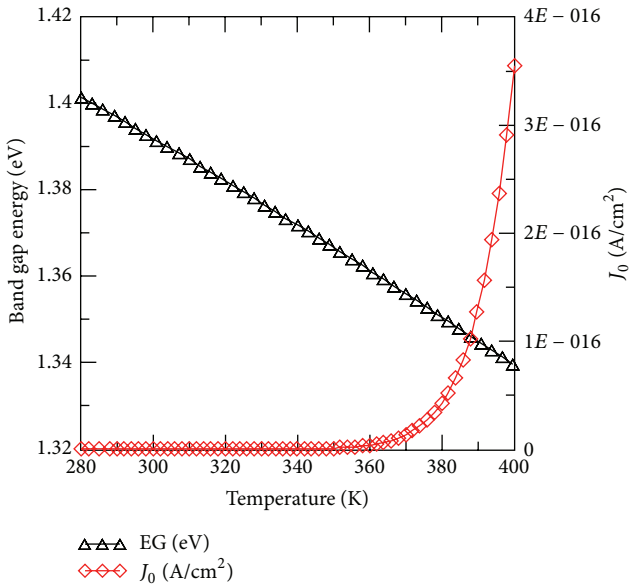

FIGURE 12: $In_{0.622}Ga_{0.378}N$ solar cell band gap and reverse saturation current density versus temperature.

cell performance was more affected by the front layer than back layer. The optimum efficiency found, under normalized conditions (AM1.5G, 0.1 W/cm^2, and 300 K), is 26.50%.

In this paper, we have also studied the effect of the minority carrier lifetime and the surface recombination velocity on the conversion efficiency of the $In_{0.622}Ga_{0.378}N$ solar cell and it was found that, to minimize the power losses, the carrier lifetime should be improved by reducing the defects density, and the surface recombination velocity should not exceed 10^3 cm·s^{-1}.

At last, we have studied the electrical characteristics fluctuation of the single-junction $In_{0.622}Ga_{0.378}N$ solar cell with the temperature variation, and we have noticed a strong performance degradation with the increasing of the temperature; this is due to the temperature dependency of the physical parameters of the solar cell.

Conflict of Interests

The authors declare that there is no conflict of interests regarding the publication of this paper.

Acknowledgment

The authors would like to thank Mr. S. Elmetnani (UDES) for his valuable advice on the writing of this paper.

References

[1] L. A. Vilbois, A. Cheknane, A. Bensaoula, C. Boney, and T. Benouaz, "Simulation of a solar cell based on InGaN," *Energy Procedia*, vol. 18, pp. 795–806, 2012.

[2] N. Akter, "Design and simulation of Indium Gallium Nitride multijunction tandem solar cells," *International Journal of Research in Engineering and Technology*, vol. 3, no. 1, pp. 315–321, 2014.

[3] D. V. P. McLaughlin and J. M. Pearce, "Progress in indium gallium nitride materials for solar photovoltaic energy conversion," *Metallurgical and Materials Transactions A: Physical Metallurgy and Materials Science*, vol. 44, no. 4, pp. 1947–1954, 2013.

[4] X. Zhang, X. Wang, H. Xiao et al., "Simulation of In0.65$Ga_{0.35}$ N single-junction solar cell," *Journal of Physics D: Applied Physics*, vol. 40, no. 23, pp. 7335–7338, 2007.

[5] X. Shen, S. Lin, F. Li et al., "Simulation of the InGaN-based tandem solar cells," in *Photovoltaic Cell and Module Technologies II*, B. von Roedern and A. E. Delahoy, Eds., vol. 7045 of *Proceedings of SPIE*, August 2008.

[6] F. Bouzid and S. Ben Machiche, "Potentials of $In_xGa_{1-x}N$ photovoltaic tandems," *Revue des Energies Renouvelables*, vol. 14, no. 1, pp. 47–56, 2011.

[7] F. Bouzid and L. Hamlaoui, "Investigation of InGaN/Si double junction tandem solar cells," *Journal of Fundamental and Applied Sciences*, vol. 4, pp. 59–71, 2012.

[8] D. Benmoussa, B. Hassane, and H. Abderrachid, "Simulation of In0.52Ga0.48N solar cell using AMPS-1D," in *Proceedings of the 1st International Renewable and Sustainable Energy Conference (IRSEC '13)*, pp. 23–26, IEEE, Ouarzazate, Morocco, March 2013.

[9] T. Zdanowicz, T. Rodziewicz, and M. Zabkowska-Waclawek, "Theoretical analysis of the optimum energy band gap of semiconductors for fabrication of solar cells for applications in higher latitudes locations," *Solar Energy Materials and Solar Cells*, vol. 87, no. 1–4, pp. 757–769, 2005.

[10] A. Mesrane, F. Rahmoune, A. Oulebsir, and A. Mahrane, "2D simulation study of $In_{0.62}Ga_{0.38}N$ solar cell structure," in *Proceedings of the 2nd International Conference on Renewable Energy (CIER '14)*, vol. 9 of *Proceedings of Engineering and Technology*, 2015.

[11] Silvaco Data System, *ATLAS User's Manual Version 5.14.0.R*, Silvaco Data System, 2013.

[12] M. Garozzo, A. Parretta, G. Maletta, V. Adoncecchi, and M. Gentili, "GaAs shallow homojunction solar cells fabricated on thin epitaxial films by a simple Zn solid state diffusion method," *Solar Energy Materials*, vol. 14, no. 1, pp. 29–49, 1986.

[13] S. M. Sze and K. K. Ng, *Physics of Semiconductor Devices*, John Wiley & Sons, Hoboken, NJ, USA, 3rd edition, 2007.

[14] S. R. Kurtz, P. Faine, and J. M. Olson, "Modeling of two-junction, series-connected tandem solar cells using top-cell thickness as an adjustable parameter," *Journal of Applied Physics*, vol. 68, no. 4, pp. 1890–1895, 1990.

[15] Z. Li, H. Xiao, X. Wang et al., "Theoretical simulations of InGaN/Si mechanically stacked two-junction solar cell," *Physica B: Condensed Matter*, vol. 414, pp. 110–114, 2013.

[16] M. Nawaz and A. Ahmad, "A TCAD-based modeling of GaN/InGaN/Si solar cells," *Semiconductor Science and Technology*, vol. 27, no. 3, Article ID 035019, 2012.

[17] J. Li, F. Li, S. Lin et al., "Theoretical study on $In_xGa_{1-x}N$/Si hetero-junction solar cells," in *Thin Film Solar Technology*, A. E. Delahoy and L. A. Eldada, Eds., vol. 7409 of *Proceedings of SPIE*, August 2009.

[18] M. Farahmand, C. Garetto, E. Bellotti et al., "Monte Carlo simulation of electron transport in the III-nitride Wurtzite phase materials system: binaries and ternaries," *IEEE Transactions on Electron Devices*, vol. 48, no. 3, pp. 535–542, 2001.

[19] G. F. Brown, J. W. Ager III, W. Walukiewicz, and J. Wu, "Finite element simulations of compositionally graded InGaN solar cells," *Solar Energy Materials & Solar Cells*, vol. 94, no. 3, pp. 478–483, 2010.

[20] J. Piprek, *Semiconductor Optoelectronic Devices: Introduction to Physics and Simulation*, Academic Press, 2003.